Optical Engineering

OpticalEngineering.SPIEDigitalLibrary.org

Comparative study of optical near-field transducers for heat-assisted magnetic recording

Anurup Datta
Xianfan Xu

SPIE.

Anurup Datta, Xianfan Xu, "Comparative study of optical near-field transducers for heat-assisted magnetic recording," *Opt. Eng.* **56**(12), 121906 (2017), doi: 10.1117/1.OE.56.12.121906.

Comparative study of optical near-field transducers for heat-assisted magnetic recording

Anurup Datta* **and Xianfan Xu**
Purdue University, School of Mechanical Engineering and Birck Nanotechnology Center, West Lafayette, Indiana, United States

Abstract. Heat-assisted magnetic recording (HAMR), widely considered to be the next generation technology for high-density data storage devices, uses a tiny plasmonic antenna called a near-field transducer (NFT) to focus light down to a subdiffraction volume. This results in a temporary and local rise in temperature of the recording medium thereby reducing its coercivity, allowing the external magnetic field to write data bits in the medium. The performance of any HAMR system strongly depends on the design of the NFT. The optical performance in terms of the optical coupling efficiency and the spot size for several different NFT designs, including the triangle antenna, E antenna, bowtie aperture, lollipop antenna, and C-aperture, are considered. Also, the corresponding temperature rise in the recording medium and the NFT is calculated and several figures of merit based on the temperature profile are compared for the different designs. This work gives a comparison of the relative performances of different types of NFT and can be a basis for choosing a suitable design for HAMR applications. [DOI: 10.1117/1.OE.56.12.121906]

Keywords: heat-assisted magnetic recording; near-field transducer; electromagnetic simulations; thermal simulations.

Paper 170478SSP received Mar. 29, 2017; accepted for publication May 4, 2017; published online May 24, 2017.

1 Introduction

To meet the demands of increased storage capacity due to the rapid growth in the digital data, the areal data density of the current data storage devices is being pushed beyond 1 Tb/in.^{2}. In the current generation hard disk drives, perpendicular magnetic recording is the predominant technology for data storage, which could allow to reach a maximum areal data density of about 500 Gbits/in.^{2}.[1] Attempts to increase the areal data density by further reducing the grain size is constrained due to the superparamagnetic limit of the medium.[2] The superparamagnetic limit relates the magnetic anisotropy of the medium and the grain size of the bits to the thermal energy of the individual bits and the criteria given in the below equation must hold for good signal-to-noise ratio

$$\frac{K_u V}{k_b T} > 70, \tag{1}$$

where K_u is the magnetic anisotropy, V is the volume of the grain, k_b is the Boltzmann constant, and T is the temperature. The thermal stability of the recording medium can be increased by increasing its magnetic anisotropy but at the same time, it also simultaneously increases the required switching magnetic field of the medium for the write cycle. Hence, one must find a proper balance between the thermal stability, writability, and the grain size to successfully scale up the areal data density. Heat-assisted magnetic recording (HAMR) promises to address this issue by raising the temperature of the medium locally.[1,3–5] With the rise in temperature of the medium, the coercivity of the medium decreases sufficiently to allow the magnetic field to write data bits in the recording medium. However, to maintain a high-density data storage, the temperature rise in the medium must be confined to a very tiny volume, in the order of tens of nanometers. Since this is much beyond the diffraction limit of visible light, conventional ways to focus light in the medium and heat it fail to achieve this resolution. In an HAMR system, a metallic nanoantenna, also known as near-field transducer (NFT), is used instead, which utilizes localized surface plasmons to concentrate and focus light to such a small volume. An external laser source is coupled to a waveguide which then transports the incident energy from the laser to the NFT. Depending on the design of the antenna and the required polarization of the light, an intense field localization near the surface of the NFT is generated. Because this surface plasmon-mediated field enhancement is a near-field phenomenon, the field diverges quickly beyond tens of nanometers. The disk spacing between the NFT and the recording medium is generally less than 5 nm, hence the NFT is able to couple the energy to the recording medium through near-field coupling.

In the visible and near-infrared wavelength range, metals are generally lossy and hence absorb a portion of the incident energy. This causes the temperature of the NFT to rise, also known as self-heating of the NFT. The temperature rise of the NFT by more than hundreds of degrees can be severely detrimental to the functionality of the NFT. At higher temperatures, the materials might become more lossy, there could be thermal-induced deformations, and reliability and thermal fatigue issues could also occur.[6–8] Hence, the temperature profile of the NFT during the operation of an HAMR system is another critical factor which should be considered while designing an NFT.

In this study, we first look at some NFT design principles and material choices and explore the existing designs which have been studied in literature. Appropriate figures of merit are introduced and discussed to quantify the performance of NFT designs. Finally, we quantitatively study the optical and

*Address all correspondence to: Anurup Datta, E-mail: datta0@purdue.edu

0091-3286/2017/$25.00 © 2017 SPIE

thermal performance of some of the widely studied NFT designs and present a qualitative discussion on the relative performance of the several NFTs.

2 Near-Field Transducer Material and Design Considerations

For a properly functional HAMR system with preferable figure of merits, the design of the NFT, the material properties as well as the working wavelength of light, are very crucial to the performance of the entire system. Typically, near-infrared wavelength (700 to 900 nm) lasers are used to excite the NFTs, primarily due to the excellent plasmonic behavior of many metals at those wavelengths and the low cost of diode lasers.

From the optical properties point of view, the material must be able to support localized surface plasmon resonance to confine and enhance the field intensity. Silver and aluminum can support localized surface plasmon in the visible region, whereas gold and copper can support it in the near-infrared region. Silver, though a better plasmonic material at the visible wavelengths and with better thermal conductivity, is generally not used due to its corrosive nature. Similarly, aluminum and copper also suffer from corrosion issues and higher losses. Hence, gold has generally been the preferred choice of material due to its highly negative real part of the dielectric constant, its high thermal conductivity, and chemical stability.[5] A numerical study by modifying the optical properties of the NFT material can give an idea about the requirements of the dielectric constant, which would provide better coupling to the recording medium and less self-heating. Apparently, a material with a low value of ε'', the imaginary part of the dielectric constant, has a low self-heating associated with it. However, to ensure proper confinement of the near-field in the recording medium, generally, a higher negative value of ε' is beneficial.[9] Recently, some transition metal nitrides, such as titanium nitrides and zirconium nitrides, have shown to be very promising plasmonic materials with superior behavior, particularly at higher temperatures.[10,11] However, gold still remains the material of choice for most of NFT designs.

From the optics point of view, the design of an NFT incorporates several strategies to achieve a tiny nanoscale optical hot spot with an enhanced field intensity. First of all, the design of NFT is made resonant at the working wavelength and is excited by the proper polarization of light, which ensures the optimal excitation of localized surface plasmons to focus beyond the diffraction limit and enhance the field intensity.[12,13] In addition, sharp features, including notches and edges, are introduced in the designs to take advantage of the lightning rod effect. The surface charge accumulates near the sharp features leading to an increase in the field intensity near the vicinity of the sharp features. It has been found that the spot size is closely related to the minimum feature size in the NFT design. Addition of an image plane also helps in the confinement of the spot size in the recording medium. The NFT design can either be aperture based where the NFT design is made out from a continuous film of metal or antenna based where the metal structure itself forms the NFT. Some of the aperture-based NFT design include the bowtie aperture,[9,14] the half bowtie aperture,[14] the C-aperture,[14,15] and the H-shaped aperture,[16] whereas the E antenna,[17,18] triangular antenna,[19] nanobeak antenna,[20] the lollipop structure,[21] and the droplet antenna[22] are some examples of the antenna-based NFTs. In this work, the performances of the triangle antenna, the bowtie aperture, the E antenna, the lollipop antenna, and the C-aperture are compared. The simulation models used in the study of these designs are described next along with the medium stack and the several figures of merit.

3 Simulation Model and Figures of Merit

Full-wave 3-D electromagnetic simulations were performed using ANSYS HFSS to study the optical performance of the different NFTs. The several layers in the media stack used in the simulation model are explained in Fig. 1. For the antenna-based NFTs, it is assumed that the NFTs were embedded in a glass substrate while for the aperture-based NFTs, a film of gold is considered on top of a glass substrate where the aperture is fabricated as shown in Figs. 1(a) and 1(b), respectively. The media stack consists of a head overcoat layer made of diamond-like carbon, a lubricant layer, air gap, medium overcoat layer, storage layer made of FePt, an interlayer made of MgO, and a heat sink layer. Except for the lollipop NFT, for the other NFTs, a Gaussian beam of diameter 600 nm was assumed to be incident on the NFT with the proper polarization. For the lollipop antenna, a parabolic waveguide was modeled and two separate wave fronts 180 deg out-of-phase were assumed to be incident on the entrance face

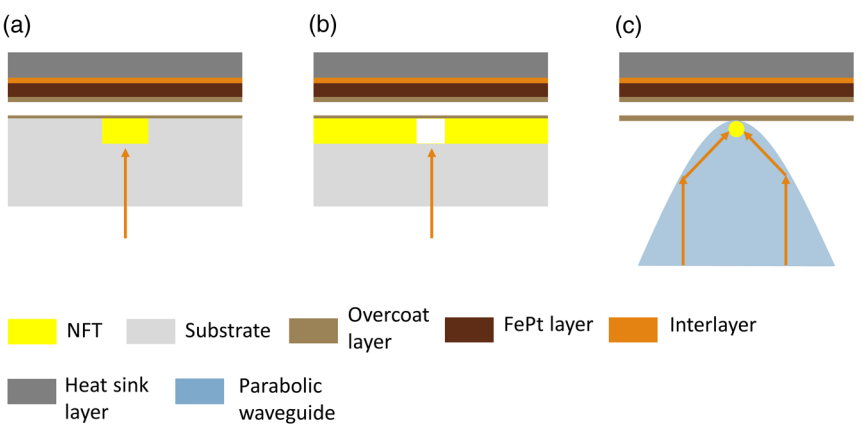

Fig. 1 Simulation models showing the different layers in the media stack for (a) an antenna-based NFT, (b) aperture-based NFT, and (c) lollipop antenna with a parabolic waveguide.

of the parabolic waveguide as explained in Ref. 21. Figure 1(c) explains the model and the excitation scheme. The absorption in the recording medium and the NFT can be calculated by the power dissipated according to the following equation:

$$q''' = \frac{1}{2}\varepsilon_0 \omega \,\mathrm{Im}(\varepsilon)|E|^2, \tag{2}$$

where ε_0 is the free-space permittivity, ω is the frequency of the light, ε is the complex permittivity of the gold, and $|E|$ is the electric field. The primary figure of merit that was used for quantifying the optical performance of the different NFTs is the coupling efficiency, which is defined as the power absorbed in the recording medium within a disk of diameter 70 nm divided by the net incident power on the NFT. In addition, the spot sizes in the recording medium are also compared across the different NFTs.

Based on the optical simulation results, subsequent thermal simulations were carried out using ANSYS Workbench. Transient thermal calculations were performed to capture the temperature rise of the medium and the NFT. The power absorbed in the recording medium and the NFT per unit volume was taken as the source term in the heat diffusion equation as

$$\rho c \frac{\partial T}{\partial t} = \frac{\partial}{\partial x}\left(k_x \frac{\partial T}{\partial x}\right) + \frac{\partial}{\partial y}\left(k_y \frac{\partial T}{\partial y}\right) + \frac{\partial}{\partial z}\left(k_z \frac{\partial T}{\partial z}\right) + q'''. \tag{3}$$

Radiation boundary condition was considered at the outer faces of the model.

For the thermal calculations, the following figures of merit were considered:

a. $\frac{\Delta T_{\text{medium}}}{\Delta T_{\text{NFT}}}$: This denotes the peak temperature rise of the recording medium to the peak temperature rise of the NFT. The temperature rise of the recording medium is calculated at the end of 1 ns, which is typically the time for which a particular region of the recording medium is heated. The NFT can either be heated in a pulsed mode or can be heated continuously and hence the NFT temperature is considered both at the end of 1 ns and at the steady state. Accordingly, the two related figures of merit are given as: $\frac{\Delta T_{\text{medium}}}{\Delta T_{\text{NFT}}|_{\text{steady state}}}$ and $\frac{\Delta T_{\text{medium}}}{\Delta T_{\text{NFT}}|_{t=1\text{ ns}}}$. The higher number for this figure of merit indicates a greater medium temperature rise for low NFT self-heating, which is beneficial for HAMR application.

b. Thermal spot size: This is the full width at half maxima of the temperature profile at the recording medium at the end of 1 ns. The thermal spot size should be as low as possible for better localization of the temperature rise.

c. Thermal gradient: The temperature change per unit length is calculated at a location which is 20 K less than the peak temperature at the recording medium. The thermal gradients are expressed for both the down- and the cross-track directions. The cross-track gradient is related to the track density while the down-track gradient determines the linear density of data. Greater thermal gradients are preferred in the recording medium, which will eliminate long thermal tails.

d. $\frac{\Delta T_{\text{medium}}}{P_{\text{incident}}}$: This denotes the overall thermal efficiency of the NFT system and is given by the temperature rise of the medium per unit incident power.

4 Results and Discussions

To have the peak performance for a particular NFT design, the dimensions of its several geometrical features have to be optimized. For each of the designs, the dimensions are described and the qualitative discussions are included about the most relevant geometrical parameters which affect the performance of the NFTs. The minimum feature size in each of the design is limited to 20 nm based on fabrication consideration and to eliminate undue lightning rod effects for smaller features. The structures are simulated at wavelengths between 700 and 900 nm depending on the dimensions and the optimum coupling efficiency and it is assumed that the incident power is 5 mW.

4.1 *Triangle Antenna*

Figure 2(a) shows a triangle antenna with a being the height of the triangle and b being the base, and the thickness (not shown in the figure) is denoted by t. The antenna generates a hot spot at the apex of the triangle when excited by a wave polarized along the longitudinal axis. Both the dimensions, a and b, affect the plasmonic modes supported by the NFT. With the increase in the length a, the resonance wavelength for the structure shifts to a longer wavelength. On the other hand, the increase in the dimension b has a lesser effect on the resonance wavelength but it affects the coupling efficiency. An optimized value of $a = 150$ nm, $b = 200$ nm, and $t = 80$ nm gives a coupling efficiency of 2.7% and a spot size of 28 nm × 40 nm. Figure 2(b) shows the absorption profile in the recording medium. It is seen that apart from the single hot spot at the tip of the triangle, there are two tiny spots near the other two vertices of the triangle. The thermal simulation results are given in Fig. 2(c) which shows the temperature profile of the recording medium at the end of 1 ns while the NFT steady-state temperature is shown in Fig. 2(d). Due to the high thermal conductivity of gold, the variation in the NFT temperature is not significant. The figures of merit, $\frac{\Delta T_{\text{medium}}}{\Delta T_{\text{NFT}}|_{\text{steady state}}}$, for the triangular antenna is 0.87 while the $\frac{\Delta T_{\text{medium}}}{\Delta T_{\text{NFT}}|_{t=1\text{ ns}}}$ is 4.9. While the temperature rise of the medium is sufficiently higher compared to the temperature of the NFT after 1 ns, when the NFT is heated continuously and allowed to reach a steady state, it can heat up more than the recording medium which is severely detrimental to the functioning of NFT. The thermal spot size is 63 nm × 76 nm, and the peak temperature rise of the medium per unit power is 74.5 K/mW. The thermal gradient in the cross-track direction is 3.49 K/nm while that for the down-track is 4.6 K/nm.

4.2 *E Antenna*

The E antenna is studied as shown in Fig. 3(a) with the relevant dimensions. The dimension of the body of the E antenna controls the resonance condition at a particular wavelength; the notch helps in achieving higher field intensity

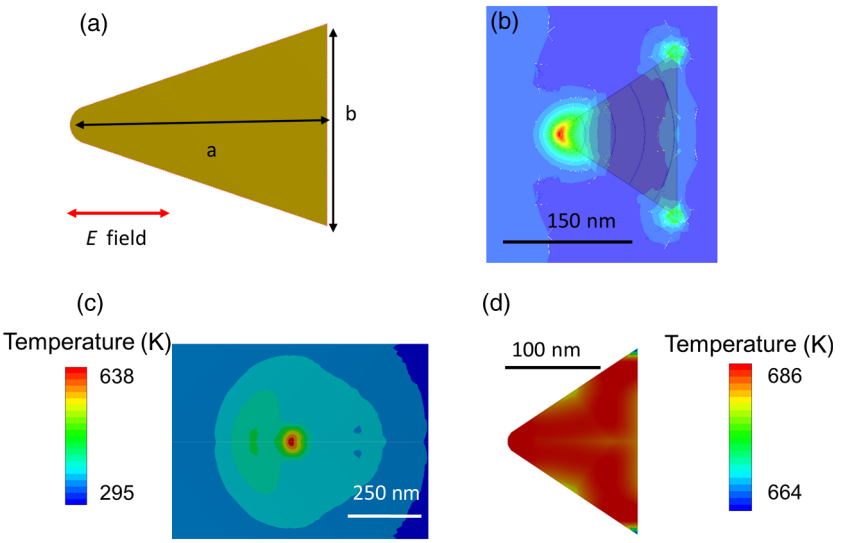

Fig. 2 (a) Dimensions of the triangle antenna, (b) absorption profile in the recording medium, (c) temperature profile in the recording medium at the end of 1 ns, and (d) temperature of the NFT at steady state.

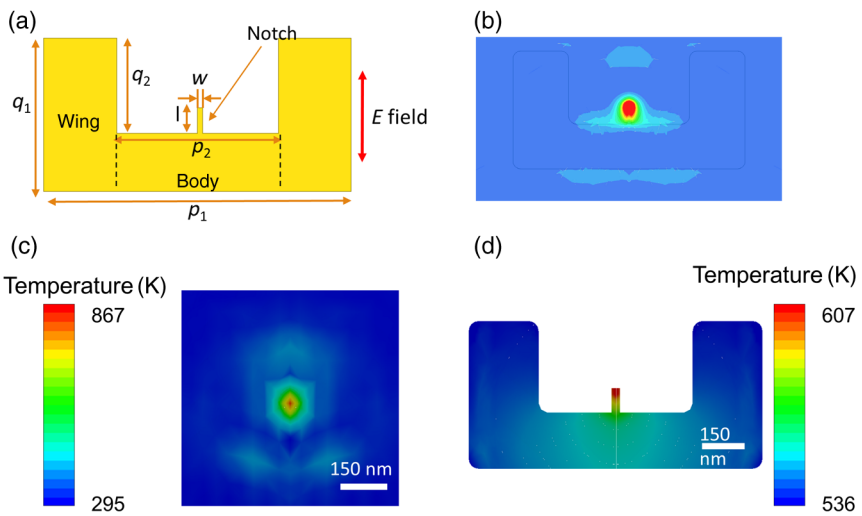

Fig. 3 (a) Relevant dimensions of the E antenna, (b) absorption profile in the recording medium, (c) temperature profile in the recording medium at the end of 1 ns, and (d) temperature of the NFT at steady state.

through the lightning rod effect, while the wings at the two sides help in funneling more surface charges to the notch. The minimum spot size in the recording medium is largely dictated by the width of the notch and considering the fabrication constraints, the notch width was limited to 20 nm in the design as mentioned earlier. Optimized dimensions of several parameters at a wavelength of 850 nm are given by: $w = 20$ nm, $l = 50$ nm, $p_1 = 600$ nm, $p_2 = 316$ nm, $q_1 = 300$ nm, and $q_2 = 186$ nm which gives a coupling efficiency of 5.8% and a spot size of 32 nm × 36 nm and the absorption profile is shown in Fig. 3(b). The thermal performance is detailed in Figs. 3(c) and 3(d) where the recording medium temperature is shown at the end of 1 ns and the steady-state NFT temperature is shown, respectively. The figure of merit, $\frac{\Delta T_{\text{medium}}}{\Delta T_{\text{NFT}}|_{\text{steady state}}}$, for the E antenna is 1.83 while the $\frac{\Delta T_{\text{medium}}}{\Delta T_{\text{NFT}}|_{t=1\text{ ns}}}$ is 7.42. Here, the steady-state NFT temperature, unlike the triangle antenna, is less than the recording medium temperature after 1 ns. The thermal spot size is 76 nm × 89 nm, and the peak temperature rise of the medium per unit power is 124.3 K/mW. The thermal gradient in the cross-track direction is 7.55 K/nm while that for the down-track is 6.76 K/nm. We see that the E antenna performs better than the triangle antenna in terms of several figures of merit, including the thermal gradient and the thermal efficiency of the NFT system.

4.3 *Lollipop Antenna*

The lollipop antenna introduced by Challener et al.[21] consists of a circular metallic disk and a peg attached to it at one side as shown in Fig. 4(a). The disk can support different resonance modes, such as dipole like, quadrapole like, or even higher modes, depending on the incident wavelength and at resonance, these modes facilitate the flow of surface charges to the peg, which provides the lightning rod effect for field enhancement and localization. The dimensions of $d = 190$ nm, $P_l = 20$ nm, $P_w = 20$ nm, $t = 35$ nm at 830-nm

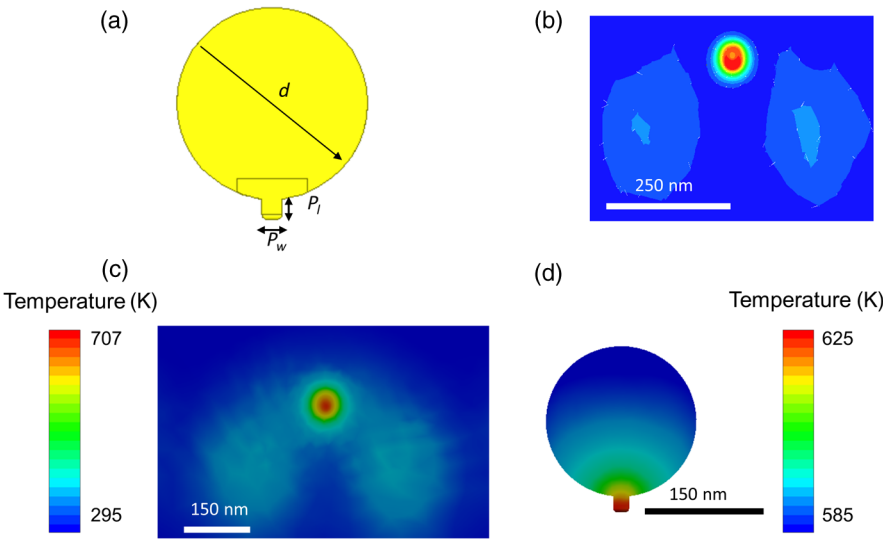

Fig. 4 (a) Relevant dimensions of the lollipop antenna, (b) absorption profile in the recording medium, (c) temperature profile in the recording medium at the end of 1 ns, and (d) temperature of the NFT at steady state.

incident wavelength generate a quadrapole excitation mode in the disk and a coupling efficiency of 3.5% is obtained. This generates a spot size of 44 nm × 51 nm in the recording medium and the absorption profile in the recording medium is shown in Fig. 4(b). Figure 4(c) shows the temperature distribution in the recording medium after 1 ns and a thermal spot size of 65 nm × 71 nm is obtained. We also notice there are two side lobes present in the recording medium which originate from the parabolic waveguide. However, the temperature in these side lobes is much less than the temperature at the central hot spot. The figures of merit, $\frac{\Delta T_{\text{medium}}}{\Delta T_{\text{NFT}}|_{\text{steady state}}}$, for this antenna is 1.24 while the $\frac{\Delta T_{\text{medium}}}{\Delta T_{\text{NFT}}|_{t=1\text{ ns}}}$ is 3.34. The peak temperature rise of the medium per unit power is 82.4 K/mW. In terms of these figures of merit, the lollipop antenna performs better than the triangle but not as good as the E antenna. The thermal gradient in the cross-track direction is 3.7 K/nm while that for the down-track is 3.14 K/nm.

4.4 *Bowtie Aperture*

Bowtie aperture is an aperture-based NFT, which is shown in Fig. 5(a). It consists of two triangular arms with a small gap in between them and the relevant parameters which define the bowtie performance are the outline dimension, x and y, the gap size, g, and the thickness, t. The smaller the gap size, the smaller is the spot size in the recording medium. The gap size is fixed at 20 nm in the current design. The bowtie aperture acts as a ridge waveguide and the outline

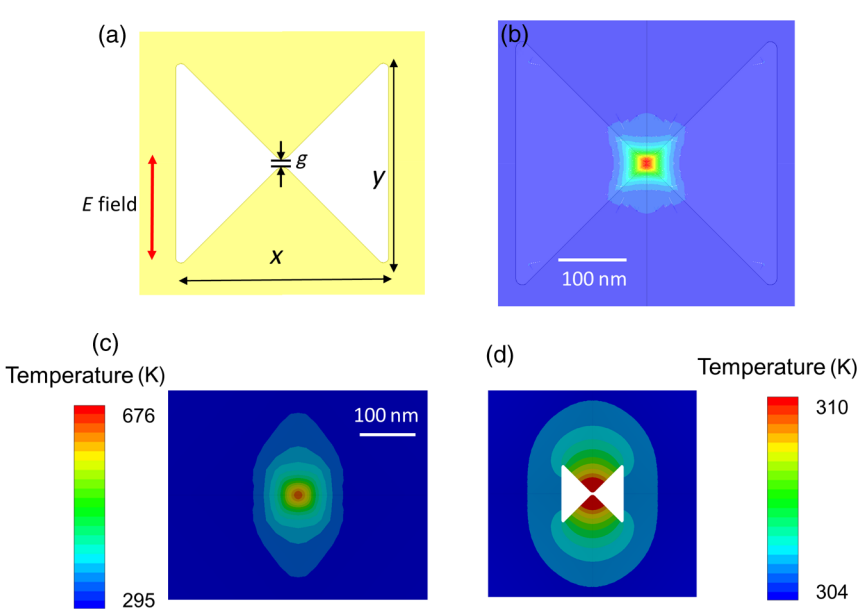

Fig. 5 (a) Relevant dimensions of the bowtie aperture, (b) absorption profile in the recording medium, (c) temperature profile in the recording medium at the end of 1 ns, and (d) temperature of the NFT at steady state.

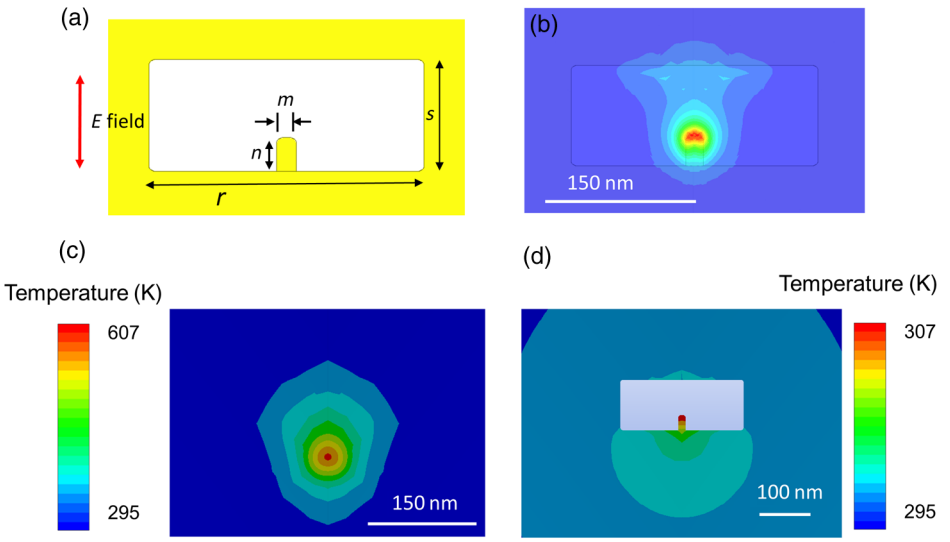

Fig. 6 (a) Relevant dimensions of the C-aperture, (b) absorption profile in the recording medium, (c) temperature profile in the recording medium at the end of 1 ns, and (d) temperature of the NFT at steady state.

dimension defines the cutoff wavelength of the aperture. At 800-nm wavelength, dimensions of $x = 400$ nm and $y = 400$ nm with a thickness of 90 nm generate a coupling efficiency of 3.2% and a spot size of 36 nm × 44 nm and the absorption profile is shown in Fig. 5(b). Figure 5(c) shows the temperature profile of the recording medium after 1 ns, which shows a peak temperature of 676 K and a spot size of 54 nm × 68 nm. The steady-state temperature of the NFT is 310 K, as seen in Fig. 5(d), which is much less than the other antenna-based NFTs. Due to the high thermal conductivity of the gold film, the heat generated at the tip of the NFT can dissipate very quickly leading to a much lower rise in temperature of the NFT. Accordingly, the thermal figures of merit, $\frac{\Delta T_{\text{medium}}}{\Delta T_{\text{NFT}}|_{\text{steady state}}}$, is 25.4 and $\frac{\Delta T_{\text{medium}}}{\Delta T_{\text{NFT}}|_{\text{t=1 ns}}}$ is 63.5. The peak temperature rise of the medium per unit power is 82.8 K/mW and the thermal gradient in the cross-track direction is 4.38 K/nm while that for the down-track is 5.44 K/nm.

4.5 *C-Aperture*

The C-aperture is another aperture-based ridge waveguide-like NFT, which consists of a rectangular window in a metal film with a notch for field concentration as shown in Fig. 6(a). The aperture portion resembles the C shape. The C-aperture closely resembles the rectangular waveguide and hence the length and breadth of the aperture are both crucial for generating and concentrating surface plasmons at the tip of the notch. At 800-nm wavelength, $s = 100$ nm, $r = 250$ nm, $m = 20$ nm, $n = 30$ nm, and a thickness of 100 nm gives a coupling efficiency of 2.6% and a spot size of 32 nm × 34 nm and the absorption profile is shown in Fig. 5(b). The temperature profile of the recording medium after 1 ns is plotted in Fig. 6(c), which shows a peak temperature of 607 K. The thermal spot size is found to be 64 nm × 76 nm. Similar to the bowtie aperture, the steady-state temperature is also quite low 307 K as seen in Fig. 6(d). The thermal figures of merit are as follows: $\frac{\Delta T_{\text{medium}}}{\Delta T_{\text{NFT}}|_{\text{steady state}}} = 26$ and $\frac{\Delta T_{\text{medium}}}{\Delta T_{\text{NFT}}|_{\text{t=1 ns}}} = 28.3$. The peak temperature rise of the medium per unit power is 67.8 K/mW and the thermal gradient in the cross-track direction is 4.15 K/nm while that for the down-track is 4.4 K/nm.

Tables 1 and 2 summarize the optical figures of merit and the thermal figures of merit for different NFT designs, respectively. From Table 1, we find that the E antenna is one of the best in terms of the coupling efficiency into the recording medium and there is not much difference in the optical spot sizes for the different designs except for the lollipop antenna, which has a slightly bigger spot size. For the lollipop antenna, the spot size depends on both the peg width and the thickness of the metal film. While the peg width is fixed at 20 nm, the film thickness of 35 nm was considered which gives a higher coupling efficiency but at the same time also increases the spot size. As mentioned earlier, from Table 2, we see that aperture-based NFTs, such as the bowtie aperture and the C-aperture, perform much better when the figure of merit $\frac{\Delta T_{\text{medium}}}{\Delta T_{\text{NFT}}}$ is considered since the heat can quickly diffuse over a larger area within the metal film leading to a low rise in the NFT peak temperature. However, from a practical point of view, the magnetic write pole also needs to be incorporated near the NFT head, which provides the required magnetic field during the write and the read cycle. The placement of the magnetic pole in a continuous film-based NFT might be challenging and needs to be addressed to exploit the benefits of having a low figure of merit of $\frac{\Delta T_{\text{medium}}}{\Delta T_{\text{NFT}}}$. It can also be observed that the trend of the

Table 1 Optical figures of merit for NFTs.

NFT design	Coupling efficiency (%)	Optical spot size
Triangle antenna	2.7	28 nm × 40 nm
E antenna	5.8	32 nm × 36 nm
Lollipop antenna	3.5	44 nm × 51 nm
Bowtie aperture	3.2	36 nm × 44 nm
C-aperture	2.6	32 nm × 34 nm

Table 2 Thermal figures of merit for NFTs.

NFT design	$\frac{\Delta T_{medium}}{\Delta T_{NFT}}$		Thermal spot size	Temperature rise per unit power (K/mW)	Thermal gradient (K/nm)	
	NFT temp at 1 ns	NFT temp at steady state			Cross-track	Down-track
Triangle antenna	4.9	0.87	63 nm × 76 nm	74.5	3.49	4.6
E antenna	7.42	1.83	76 nm × 89 nm	124.3	7.55	6.46
Lollipop antenna	3.34	1.24	65 nm × 71 nm	82.4	3.7	3.14
Bowtie aperture	63.5	25.4	54 nm × 68 nm	82.8	4.38	5.44
C-aperture	28.3	26	64 nm × 76 nm	67.8	4.1	4.4

temperature rise per unit power is very closely related to the coupling efficiency across the different designs. The differences in the thermal spot size are related to both the optical spot size and the shape of the spot. The anisotropic thermal conductivity of the recording medium (in-plane thermal conductivity: 1.5 W/mK and out-of-plane thermal conductivity: 7 W/mK) helps in restricting the diffusion of the heat laterally and more heat is diffused in the vertical direction, which helps in ensuring a smaller spot size in the recording medium. This also affects the thermal gradient values. Tailoring the thermal spot size or the thermal gradient can be done either by modifying the optical spot profile by innovative NFT designs or by adjusting the layers above and below the storage layer, such as by introducing high conductivity heat sink layer or low-thickness interlayer.

5 Conclusion

Comparisons among different NFT designs, such as the triangle antenna, the E antenna, the lollipop antenna, the bowtie aperture, and the C–aperture, are presented. Optical and thermal simulations results are presented and different figures of merit are described to quantify the performance of the different designs. It has been found that among the antenna-based NFTs, E antenna has one of the best performances. Also, it is seen that aperture-based NFTs have significantly less NFT self-heating compared to the antenna-based designs. Finding ways to incorporate them in an actual HAMR design would be very useful in improving the performance. This work can serve as a basis for evaluating different designs for use in the HAMR system.

Acknowledgments

Support to this work by the Advanced Storage Technology Consortium is acknowledged. The authors would like to thank Zhou Zeng for his help in some of the simulations. The authors declare no conflict of interest.

References

1. R. E. Rottmayer et al., "Heat-assisted magnetic recording," *IEEE Trans. Magn.* **42**(10), 2417–2421 (2006).
2. M. P. Sharrock, "Time-dependent magnetic phenomena and particle-size effects in recording media," *IEEE Trans. Magn.* **26**(1), 193–197 (1990).
3. M. H. Kryder et al., "Heat assisted magnetic recording," *Proc. IEEE* **96**, 1810–1835 (2008).
4. L. Pan and D. B. Bogy, "Data storage: heat-assisted magnetic recording," *Nat. Photonics* **3**, 189–190 (2009).
5. N. Zhou et al., "Plasmonic near-field transducer for heat-assisted magnetic recording," *Nanophotonics* **3**(3), 141–155 (2014).
6. B. Xu et al., "Thermal issues and their effects on heat-assisted magnetic recording system," *J. Appl. Phys.* **111**(7), 07B701 (2012).
7. B. Liu and Y. Han, "Writing induced nanodeformation and its effects on head-disk clearance," *J. Appl. Phys.* **93**(10), 8716–8718 (2003).
8. H. Reddy et al., "Temperature-dependent optical properties of gold thin films," *Opt. Mater. Express* **6**(9), 2776–2802 (2016).
9. N. Zhou, L. M. Traverso, and X. Xu, "Power delivery and self-heating in nanoscale near field transducer for heat-assisted magnetic recording," *Nanotechnology* **26**(13), 134001 (2015).
10. G. V. Naik, V. M. Shalaev, and A. Boltasseva, "Alternative plasmonic materials: beyond gold and silver," *Adv. Mater.* **25**(24), 3264–3294 (2013).
11. P. R. West et al., "Searching for better plasmonic materials," *Laser Photonics Rev.* **4**(6), 795–808 (2010).
12. L. Wang and X. Xu, "Spectral resonance of nanoscale bowtie apertures in visible wavelength," *Appl. Phys. A* **89**, 293–297 (2007).
13. L. Novotny and N. Van Hulst, "Antennas for light," *Nat. Photonics* **5**(2), 83–90 (2011).
14. N. Zhou, E.C. Kinzel, and X. Xu, "Nanoscale ridge aperture as near-field transducer for heat-assisted magnetic recording," *Appl. Opt.* **50**(31), G42–G46 (2011).
15. X. Shi and L. Hesselink, "Mechanisms for enhancing power throughput from planar nano-apertures for near-field optical data storage," *Jpn. J. Appl. Phys.* **41**(3S), 1632–1635 (2002).
16. E. Jin and X. Xu, "Radiation transfer through nanoscale apertures," *J. Quant. Spectrosc. Radiat. Transfer* **93**(1–3), 163–173 (2005).
17. B. C. Stipe et al., "Magnetic recording at 1.5 Pb m^{-2} using an integrated plasmonic antenna," *Nat. Photonics* **4**(7), 484–488 (2010).
18. A. Datta and X. Xu, "Improved near field transducer design for heat assisted magnetic recording," *IEEE Trans. Magn.* **52**(12), 1–6 (2016).
19. W. A. Challener and A. V. Itagi, "Near-field optics for heat-assisted magnetic recording (experiment, theory, and modeling)," in *Modern Aspects of Electrochemistry, Modelling and Numerical Simulations II*, M. Schlesinger, Ed., Vol. 44, pp. 53–111, Springer, New York (2009).
20. T. Matsumoto et al., "Integrated head design using a nanobeak antenna for thermally assisted magnetic recording," *Opt. Express* **20**(17), 18946 (2012).
21. W. Challener et al., "Heat-assisted magnetic recording by a near-field transducer with efficient optical energy transfer," *Nat. Photonics* **3**(4), 220–224 (2009).
22. J. Gosciniak et al., "Novel droplet near-field transducer for heat-assisted magnetic recording," *Nanophotonics* **4**(4), 503–510 (2015).

Anurup Datta is a PhD student in the Department of Mechanical Engineering at Purdue University. He received his BTech degree in manufacturing science and engineering from Indian Institute of Technology, Kharagpur, in 2012. His research interests include sub-wavelength focusing of light, nanolithography, and heat-assisted magnetic recording. He is a student member of SPIE.

Xianfan Xu is the James J. and Carol L. Shuttleworth professor of mechanical engineering at Purdue University. He is the recipient of the National Science Foundation Faculty CAREER Award, the Office of Naval Research Young Investigator Award, and the ASME Heat Transfer Memorial Award. His research interests include ultrafast laser–matter interaction, nano-optics, and laser-based micro, and nanoengineering. He is a fellow of SPIE and a fellow of the American Society of Mechanical Engineers.